Design of A 50-kW Medium Frequency Medium Voltage Transformer for 10-kV SiC-Based Dual Active Bridge Converter

2023 IEEE Energy Conversion Congress and Exposition (ECCE) | 979-8-3503-1644-5/23/$31.00 ©2023 IEEE | DOI: 10.1109/ECCE53617.2023.10362890

Zihan Gao
Min H. Kao Department of Electrical Engineering and Computer Science
The University of Tennessee, Knoxville
Knoxville, TN, USA
zgao15@vols.utk.edu

Dingrui Li
Min H. Kao Department of Electrical Engineering and Computer Science
The University of Tennessee, Knoxville
Knoxville, TN, USA
dli35@vols.utk.edu

Ruirui Chen
Min H. Kao Department of Electrical Engineering and Computer Science
The University of Tennessee, Knoxville
Knoxville, TN, USA
rchen14@vols.utk.edu

Hua Bai
Min H. Kao Department of Electrical Engineering and Computer Science
The University of Tennessee, Knoxville
Knoxville, TN, USA
hbai2@utk.edu

Leon Tolbert
Min H. Kao Department of Electrical Engineering and Computer Science
The University of Tennessee, Knoxville
Knoxville, TN, USA
tolbert@utk.edu

Fred Wang
Min H. Kao Department of Electrical Engineering and Computer Science
The University of Tennessee
Knoxville, TN, USA
Oak Ridge National Laboratory
Oak Ridge, TN, USA
fred.wang@utk.edu

***Abstract*— In this paper, a 50-kW 1-kV/6.25-kV medium voltage dual-active-bridge (DAB) transformer has been designed and tested. The shell-type transformer structure with stacked small cores is selected to integrate the leakage inductance and reduce the eddy current loss. Dry-type insulation with selective shielding is adopted and both winding-to-ground and winding turn-to-turn insulation are considered. The transformer geometry-based design procedure is discussed to achieve high efficiency and power density considering the effect of eddy current loss and insulation constraint. Tests up to the full voltage and power were performed and the DAB transformer achieved 99.66% full-load efficiency and 13.5 kW/L density for the transformer.**

Keywords—Dual-active-bridge (DAB) converters, transformers, medium voltage

I. Introduction

Medium voltage (MV) SiC devices with high blocking voltage and fast switching speed have enabled more compact and efficient MV power conversion [1-3]. The high power and voltage capability is favorable to ac and dc grid applications [4-9]. As the dc blocking voltage of the devices increases, fewer stages are needed for MV power conversion. With the faster switching devices, the switching frequency of the converter can be increased so that the volume of passive components, i.e., inductors, transformers, capacitor banks, etc., can be shrunk [10]. In the meantime, low-loss and high saturation nanocrystalline materials make the design of MV transformers smaller whereas the efficiency is not compromised [11].

However, as the voltage goes higher, new issues such as insulation and parasitics have become the bottleneck [12]. As the voltage within and between windings increases, oil- or dry-type insulation is necessary instead of relying on air and wire coating insulation [13]. In [14], dry-type insulation has been used to achieve the partial discharge (PD) free insulation required for 4.16 kV. As encapsulated dry-type insulation demands high vacuum process and vacuum potting equipment to achieve void-free and PD-free insulation, PCB windings can be fabricated, and the PCB substrate serves as the insulation barrier [15]. Since dielectric materials are used in dry-type insulation, the electric field adjacent to windings can induce higher compared to those windings in the air. Hence, the parasitic capacitance between windings contributes to the common-mode capacitances in the converter and may cause loss and electromagnetic interference issues [16, 17].

Leakage integration can also cause eddy current loss in nanocrystalline ribbon-based cores which is not able to be

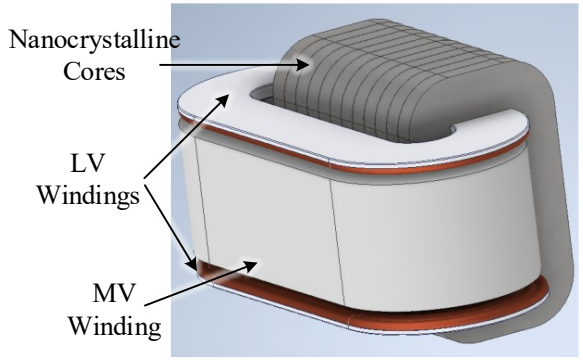

Fig. 1. Structure of MV DAB transformer.

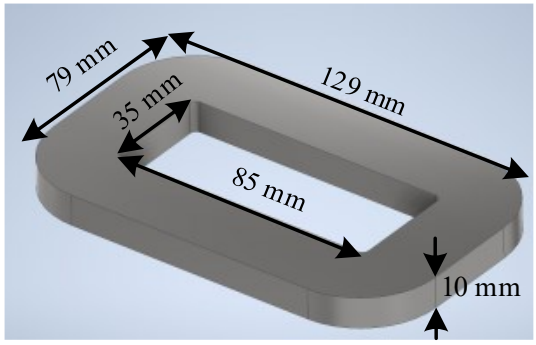

Fig. 2. Dimension of nanocrystalline-based transformer core

suppressed by ordinary laminations [18]. Therefore, to achieve an efficient and compact design, care should be taken to avoid the aforementioned issues. Ref [18] used ferrite shielding to cover the lamination surface, yet the eddy current loss reduction is not complete and the ferrite shielding layer also takes space inside the core window area. To limit the eddy current loss, [16] used smaller cores to limit the surface area of ribbon cores, and added ferrite bridges to direct the leakage field into ferrites, limiting the eddy current loss and achieving low-loss leakage integration. However, ferrite structures can also block air convection path, causing obstacles to cooling.

In this paper, a transformer design optimized for dual-active-bridge (DAB) converter rated at 50 kW, 1 kV/6.25 kV with 10-kV SiC devices have been introduced, and the design procedure considering both insulation and low loss leakage integration is proposed. In Section II, the magnetic design with low-loss leakage integration is discussed. Section III demonstrates the design validation considering insulation and eddy current loss. Section IV shows the MV DAB test results with the designed transformer. Section V concludes the paper.

II. Magnetic Design with Low-Loss Leakage Inductance Integration

A. Transformer Structure

Due to the operational behavior of the DAB converter, a series-connected inductor is needed for output power control and zero-voltage switching (ZVS) resonance. In MV converters, considering the high demand on insulation for both the power stage and transformer itself, leakage integration is desirable to maintain a reasonable converter volume. However, as the leakage flux may cross the lamination layer and cause eddy current loss, the transformer structure needs to be designed so as to suppress the loss. To avoid high eddy current loss, the transformer uses vertical shell-type structure to reduce excess leakage field (see Fig. 1). Also, a strategy of forming the transformer core by stacking thin cores is used. In this case, the lamination surface layer will be minimized without complicated structures, creating further "lamination" on the nanocrystalline ribbon surface to limit the eddy current [16]. The thinner the ribbon width is, the more effective eddy current limiting can be achieved. However, the width of nanocrystalline ribbon is also constrained by the manufacturability and cost. Considering the availability of manufacturers, the nanocrystalline core with ribbon width of 10 mm is selected, as shown in Fig. 2, to be stacked to form the large transformer core.

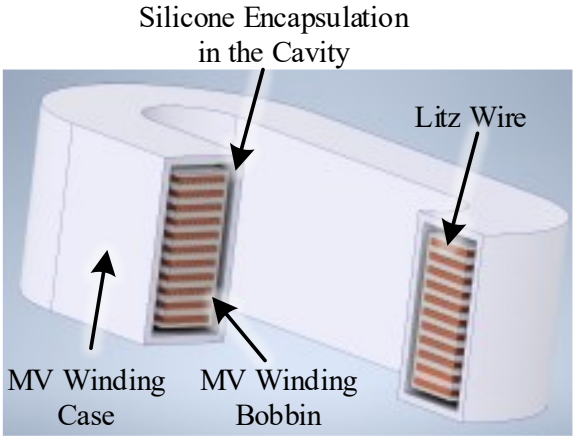

Fig. 3. Structure of MV winding with 3D printed case and dry-type insulation.

B. Transformer Insulation

As the voltage rating of the transformer is 6.25 kV on the MV side, the winding insulation needs to be considered. To achieve a compact design and reduce thermal stress, dry-type insulation for the MV winding is selected. For the ease of cooling and insulation design, only the MV winding is encapsulated with dry-type insulation, while the LV winding and transformer core are exposed to the air. Therefore, only the heat generated by the MV winding needs to be dissipated across the solid insulation material, which has low thermal conductivity.

The MV winding is comprised of three parts, i.e., the Litz wire, the 3D printed winding case and bobbin, and the silicone elastomer filled inside the winding cavity [19], which is illustrated in Fig. 3. In order to confine the electric field inside of the MV winding and avoid discharge onto the other components, the MV winding is selectively shielded with conductive coating on the surfaces facing the transformer core and LV windings [16].

C. Transformer Geometry Optimization

With the main structure and basic core element selected, the transformer can be optimized to achieve the desired performance. The transformer design procedure mainly determines the transformer core stacking numbers, MV/LV Litz wire gauges, and winding turn numbers. The voltage and power ratings, as mentioned, are 1 kV/6.25 kV 50 kW, respectively. The switching frequency is set at 10 kHz, which is limited due to the switching loss performance and gate drive capability of 10 kV SiC devices.

The main constraint on the core window geometry is shown in Fig. 4. Among the dimensions, H represents the window height, W the window width, D_{LV} and D_{MV} the diameters of LV/MV Litz wires. As the dielectric constants of silicone encapsulation and 3D printing material used are close, the dry-type insulation is considered homogeneous here, so d_s is the thickness of dry-type insulation on the MV winding, d_{ry} the

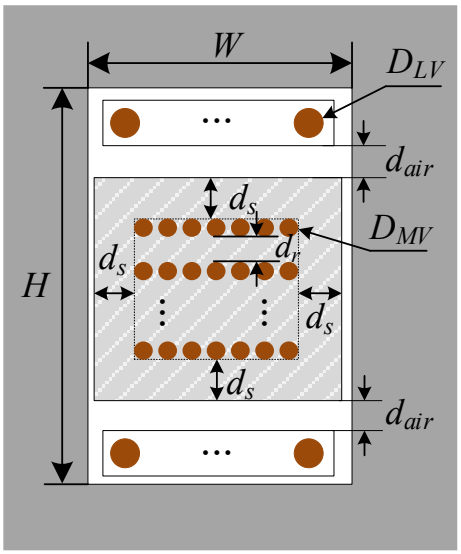

Fig. 4. Geometry constraint of windings in the core window of MV transformer.

insulation thickness between each layer of MV winding. d_{air} is the clearance between MV and LV windings for cooling air channel and leakage integration. Therefore, the geometry constraint can be obtained as

$$N_{r,LV}D_{LV} + 2d_s + 2d_{air} + N_{r,MV}D_{MV} < H \tag{1}$$

where, $N_{r,LV}$, $N_{r,MV}$ are the row numbers of LV and MV windings, respectively, which can be found as

$$\begin{cases} N_{r,LV} = \left\lceil N_{LV} \Big/ \left\lfloor \frac{W}{D_{LV}} \right\rfloor \right\rceil \\ N_{r,MV} = \left\lceil N_{MV} \Big/ \left\lfloor \frac{W - 2d_s}{D_{LV}} \right\rfloor \right\rceil \end{cases} \tag{2}$$

where $\lfloor\cdot\rfloor$ represents the floor function, $\lceil\cdot\rceil$ the ceiling function, and N_{MV}, N_{LV} are the turns number of MV/LV windings, respectively. With the geometry constraint determined, the winding turns wound inside the core window can be found.

The numbers of small nanocrystalline cores, as another design variable, defines the core cross-sectional area and mean length turn (MLT) of the windings, and therefore affects the core and winding losses. The relationships between the core stacking number, the core cross-sectional area and the MLT are,

$$\begin{cases} A_{core,tot} = N_{stack}A_{core} \\ \text{MLT} = 2N_{stack}d_{core} + \pi D_{winding} \end{cases} \tag{3}$$

where, $A_{core,tot}$ and A_{core} are the cross-sectional areas of the whole transformer core and each thin core element, N_{stack} the number of core stacking, d_{core} the depth of each core element (10 mm), and $D_{winding}$ the center diameter of the round corner of the LV/MV racetrack winding.

To derive the current waveform for loss estimation, the transformer leakage inductance (referred to LV side) can be roughly estimated as

$$L_k = 2\left(\frac{N_{LV}}{2}\right)^2 \rho_G \mu_0 \frac{A_{gap}}{W} \tag{4}$$

where, the μ_0 is the vacuum permeability, ρ_G the Rogowski factor [20, 21].

$$\rho_G = 1 - \frac{1 - e^{\pi\left(\frac{W}{D_{LV}{}^{N_{r,LV}}/_2 + d_{air} + d_s + D_{MV}{}^{N_{r,MV}}/_2}\right)}}{\pi\left(\frac{W}{D_{LV}{}^{N_{r,LV}}/_2 + d_{air} + d_s + D_{MV}{}^{N_{r,MV}}/_2}\right)} \tag{5}$$

And, A_{gap} is the equivalent cross sectional area for leakage field of each air gap between LV and MV windings.

$$A_{gap} = N_{stack}d_{core}\left(D_{LV}\frac{N_{r,LV}}{6} + d_{air} + D_{MV}\frac{N_{r,MV}}{6}\right) \tag{6}$$

As mentioned before, the leakage inductance can induce extra eddy current loss on transformer cores. However, no analysis method is available to estimate the eddy current loss. Hence, simulation will be performed in Section III.A. to evaluate the eddy current loss for the optimized transformer.

With the geometry, core area and MLT determined, the core loss and winding loss can be calculated. The core loss can be characterized by several methods in the literature [22], and here the nanocrystalline loss (without eddy current loss) is estimated from the datasheet and iGSE method. The copper loss is calculated as the simplified Litz wire model in [23]. As the switching frequency and devices are already determined, the power stage associated conduction loss and switching losses can also be calculated. The total volume and power density can, therefore, be estimated, too.

By using a genetic algorithm to optimize the power density and efficiency, the optimization results are shown in Table I. The efficiency is estimated to be 99.6% and the power density of 13.5 kW/L can be achieved.

TABLE I. OPTIMIZATION RESULT OF THE MV TRANSFORMER

Parameters	***Values***	***Parameters***	***Values***
Power Rating	50 kW	d_{air}	7 mm
Voltage Rating	1000/6250 V	d_r	2.2 mm
Switching Frequency	10 kHz	$N_{r,MV}$	10
Stacked Core, N_{stack}	12	Core Loss	110 W
LV Winding	12 turns of 835/36 Litz wire	Copper Loss	53 W
MV Winding	75 turns of 150/36 Litz wire	Eddy Current Loss	22 W
Leakage Inductance	65 μH (referred to LV side)	Total Loss	185 W
Peak Flux Density	0.92 T	Efficiency	99.6%
d_s	7 mm	Power Density	13.5 kW/L

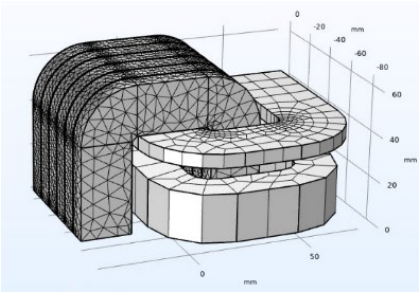

Fig. 5. Quarter-structure of stacked core transformer

III. Simulation Validation of Transformer Design

A. Transformer Eddy Current Loss Simulation

A quarter model of the designed transformer is depicted in Fig. 5. The transformer cores are modeled homogenized as in [24] and simulation of leakage flux induced eddy current is shown in Fig. 6. As the total depth of the combined core is sufficient, the leakage inductance is estimated as 62 µH, which satisfies the requirement without any ferrite structure. The calculated eddy current loss is 23 W, which is acceptable for the transformer compared with the power rating of 50 kW.

B. MV Winding Insulation Verification

In Fig. 7, within the solid winding the hot spot is at 5 kV/mm, which is below the dielectric strength of both 3D printing material and the silicone elastomer, of which the dielectric strengths are 30 kV/mm and 24 kV/mm. For the non-shielded surfaces, the electric field goes beyond the outer surface and into

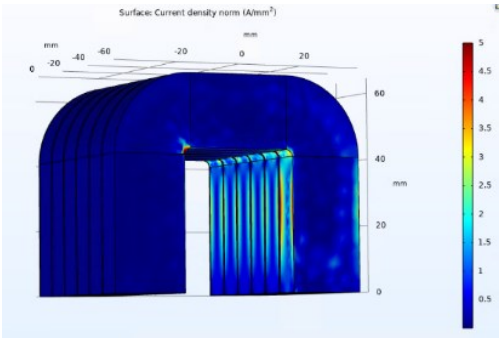

Fig. 6. Simulation result of eddy current induced by leakage field with stacked transformer core.

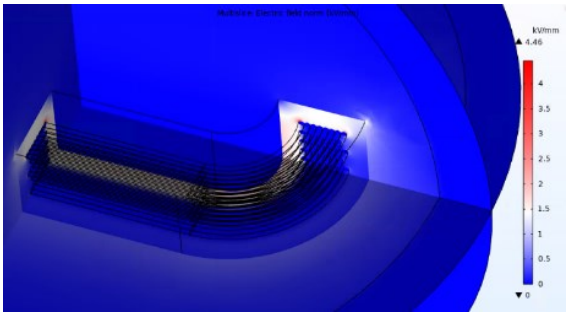

Fig. 7. Electric field simulation of MV winding.

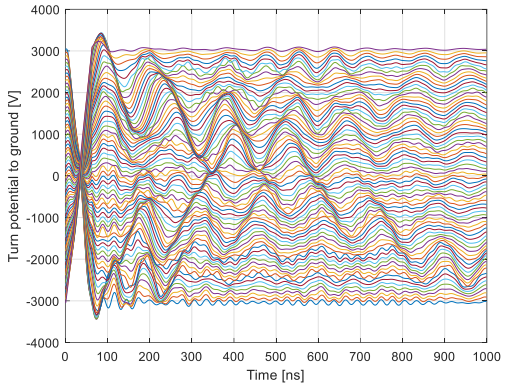

Fig. 8. Simulation result of potentials of MV winding turns.

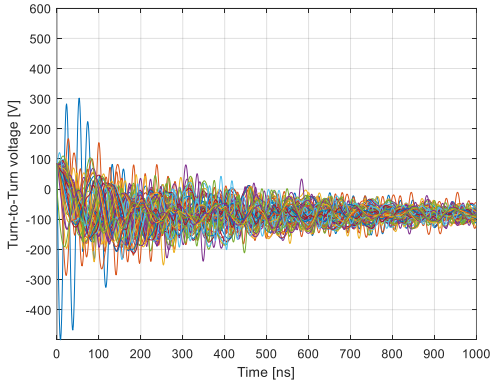

Fig. 9. Simulation result of turn-to-turn voltage in MV winding.

the air and has a field strength of 1.5 kV/mm, which is also below the dielectric strength of the air (3 kV/mm).

To verify the turn-to-turn insulation, the parasitics of each turn of the MV winding have been extracted, and the state-space model of the MV winding is constructed similar to [25]. The voltage of each turn is calculated with the switching transient. As shown in Fig. 8 and Fig. 9, the winding has transient that propagates from the outer turns to the inner turns, and the outer turns need to withstand higher voltage and oscillation, which aligned with the winding theory. The highest voltage between turns is ~500 V, which can be blocked by the Litz wire polyurethane enamel layer and the silicone elastomer encapsulation.

IV. Experimental Result of Transformer Prototype

After the transformer design has been optimized, the transformer is assembled as shown in Fig. 10(a). The transformer volume is measured as 3.7 L, with the transformer power density of 13.5 kW/L.

A. PD Test

To verify the design transformer several tests have been performed. First, the PD test was performed to verify the MV winding insulation design, and the test result is shown in Fig. 11. The PD onset voltage is tested as 7.8 kVrms/60Hz sinusoidal waveform, which corresponds to an 11 kV peak value. The PD

(a)

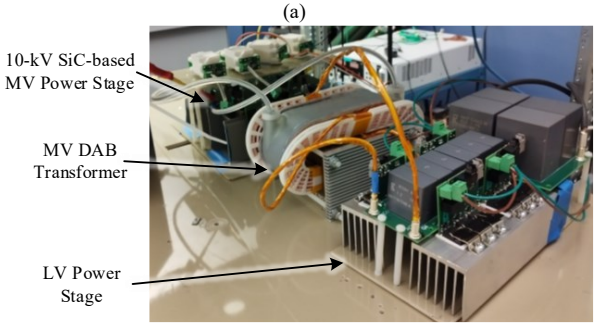

(b)

Fig. 10. Photograph of the (a) assembled MV DAB transformer, and (b) MV DAB converter.

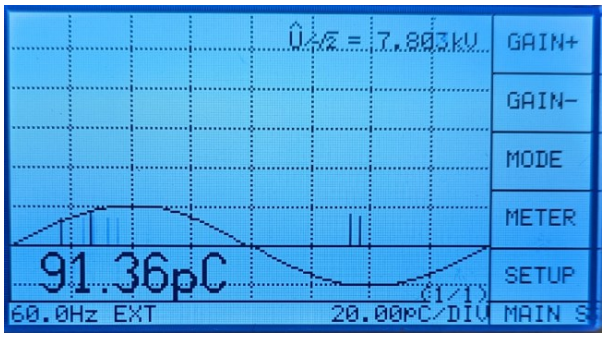

Fig. 11. PD test result of the MV DAB transformer.

performance for the assembled winding is limited by the quality of defects found during the transformer encapsulation and shielding terminations.

B. DAB Test

With verified insulation test, the MV DAB (as in Fig. 10(b)) with transformer has been tested up to the full voltage and full load. Fig. 12 shows the test waveform at full load and different power directions. Efficiency has been recorded and is as in Fig. 13. The waveform has validated the DAB performance with the transformer, and the efficiency is above 99% from LV to MV sides, and the peak efficiency is up to 99.3% at 40 kW.

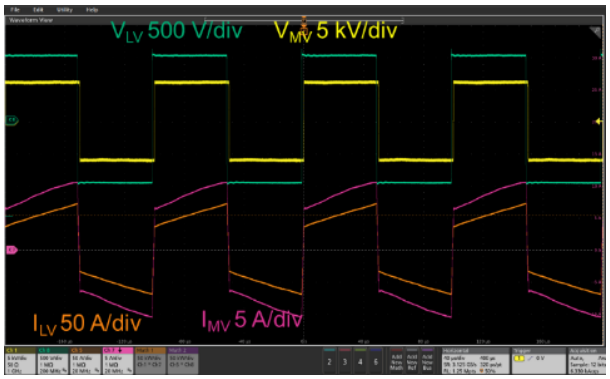

(a)

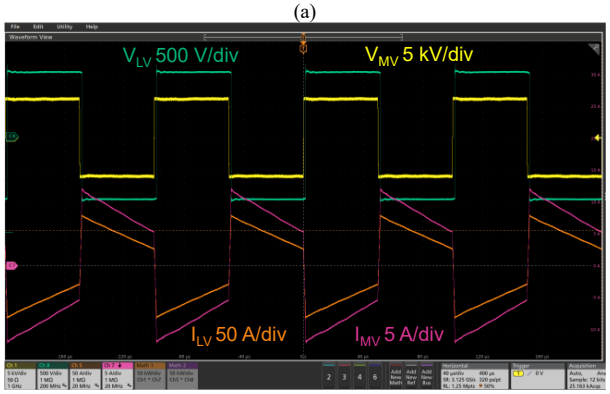

(b)

Fig. 12. Full load test waveform of DAB transformer voltages and currents: (a) from LV side to MV side, (b) from MV side to LV side.

To further investigate the loss composition of the transformer, the DAB switching frequency is swept from 10 kHz to 20 kHz, as different loss components vary differently with frequency shift. The estimated loss breakdown is shown in Fig. 14. In Fig. 14, the total loss is the recorded test result, and breakdown estimated by the transformer and DAB models. Among the different parts, the core loss, copper loss, and eddy loss are the losses associated with the transformer, and at 10 kHz, the total transformer loss is 186 W (efficiency of 99.66%), which also validates the efficiency of the transformer. The transformer volume is measured as 3.7 L, with the transformer power density of 13.5 kW/L.

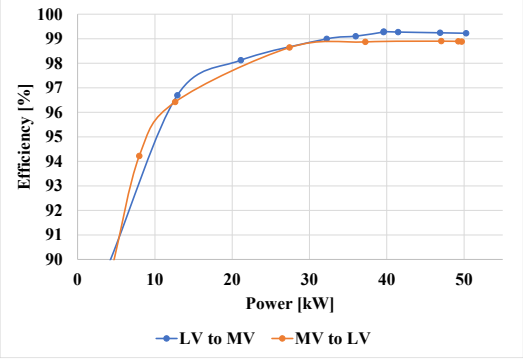

Fig. 13. Tested efficiency curve of the MV DAB converter.

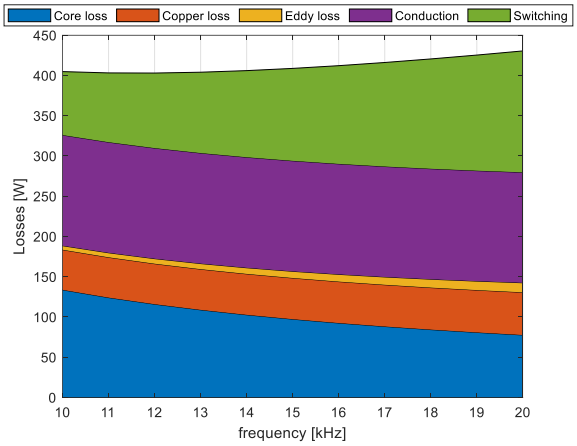

Fig. 14. Estimated MV DAB loss breakdown with sweeped switching frequency.

V. Conclusion

In this paper, a 50-kW, 1-kV/6.25-kV DAB transformer has been designed and built. The magnetic structure with low-loss leakage integration and winding insulation to the ground and inter-turns have been considered. The DAB with designed transformer has been evaluated to the full voltage and power, achieving efficiency of 99.66% and power density of 13.5 kW/L. The analysis and test validate the transformer design with stacked transformer cores, which achieves sufficient insulation capability, high efficiency and power density, providing a promising solution for MV DAB converter applications.

Acknowledgment

This work was supported primarily by the Advanced Manufacturing Office (AMO), United States Department of Energy (DOE), under Award no. DE-EE0009134. This work made use of the shared facilities of the Engineering Research Center Program of the National Science Foundation and the Department of Energy under NSF Award no. EEC-1041877.

References

[1] Z. Li, C. Zhao, Y. H. Hsieh, and Q. Li, "Partial Fluctuating Power Control of Resonant Converter for Solid-State Transformer," in *2022 IEEE Applied Power Electronics Conference and Exposition (APEC)*, 20-24 March 2022, pp. 770-776.

[2] X. Liu *et al.*, "FPGA-Based Forced Air-Cooled SiC High-Power-Density Inverter for Electrical Aircraft Applications," in *2023 IEEE Applied Power Electronics Conference and Exposition (APEC)*, 19-23 March 2023, pp. 3169-3173.

[3] H. Li, Z. Gao, and F. Wang, "Design and Demonstration of an 850 V dc to 13.8 kV ac 100 kW Three-phase Four-wire Power Conditioning System Converter Using 10 kV SiC MOSFETs," in *2023 IEEE Applied Power Electronics Conference and Exposition (APEC)*, 19-23 March 2023, pp. 989-994.

[4] X. Dong and H. Li, "A PLL-Less Voltage Sensorless Direct Deadbeat Control for a SiC Grid-Tied Inverter With LVRT Capability Under Wide-Range Grid Impedance," *IEEE Transactions on Power Electronics,* vol. 38, no. 8, pp. 9469-9481, Aug. 2023.

[5] Q. Huang *et al.*, "Islanding Detection Methods Based on Self-oscillation of Particular Frequency in DC Distribution Systems," in *2020 IEEE Applied Power Electronics Conference and Exposition (APEC)*, 15-19 March 2020, pp. 574-580.

[6] Y. He *et al.*, "Control Development and Fault Current Commutation Test for the EDISON Hybrid Circuit Breaker," *IEEE Transactions on Power Electronics,* vol. 38, no. 7, pp. 8851-8865, July 2023.

[7] H. Chen, Q. Huang, W. Li, X. Xiang, H. Luo, and X. He, "An Impedance-Based Islanding Detection Method for DC Microgrids with multiple DGs," in *2020 4th International Conference on HVDC (HVDC)*, 6-9 Nov. 2020, pp. 1025-1030.

[8] H. Chen *et al.*, "An impedance-based islanding detection method for DC microgrid with multiple distributed generators," *CSEE Journal of Power and Energy Systems,* pp. 1-16, 2022.

[9] Q. Huang, H. Chen, X. Xiang, C. Li, W. Li, and X. He, "Islanding Detection With Positive Feedback of Selected Frequency for DC Microgrid Systems," *IEEE Transactions on Power Electronics,* vol. 36, no. 10, pp. 11800-11817, Oct. 2021.

[10] D. Rothmund, T. Guillod, D. Bortis, and J. W. Kolar, "99% Efficient 10 kV SiC-Based 7 kV/400 V DC Transformer for Future Data Centers," *IEEE Journal of Emerging and Selected Topics in Power Electronics,* vol. 7, no. 2, pp. 753-767, June 2019.

[11] M. Gao, L. Yi, and J. Moon, "Mathematical Modeling and Validation of Saturating and Clampable Cascaded Magnetics for Magnetic Energy Harvesting," *IEEE Transactions on Power Electronics,* vol. 38, no. 3, pp. 3455-3468, March 2023.

[12] Z. Guo, H. Li, P. Cheetham, and N. Guvvala, "Partial Discharge Characterization of Solid-Dielectric-Based Transformer Under High Frequency High dv/dt PWM Voltage for MV Applications," in *2023 IEEE Applied Power Electronics Conference and Exposition (APEC)*, 19-23 March 2023, pp. 301-305.

[13] Z. Guo *et al.*, "A Novel High Insulation 100 kW Medium Frequency Transformer," *IEEE Transactions on Power Electronics,* vol. 38, no. 1, pp. 112-117, Jan. 2023.

[14] Z. Li, E. Hsieh, Q. Li, and F. C. Lee, "High-Frequency Transformer Design With Medium-Voltage Insulation for Resonant Converter in Solid-State Transformer," *IEEE Transactions on Power Electronics,* vol. 38, no. 8, pp. 9917-9932, Aug. 2023.

[15] R. Wang, Z. Shen, C. Zhang, B. Zhang, and P. Barbosa, "Planar Structure High-Frequency Transformer Design for Medium Voltage Applications," in *2022 IEEE Energy Conversion Congress and Exposition (ECCE)*, 9-13 Oct. 2022, pp. 1-6.

[16] Z. Gao, H. Li, and F. Wang, "A Medium-Voltage Transformer with Integrated Leakage Inductance for 10 kV SiC-Based Dual-Active-Bridge Converter," in *2022 IEEE 9th Workshop on Wide Bandgap Power Devices & Applications (WiPDA)*, 7-9 Nov. 2022.

[17] Q. Huang, Y. Yang, Z. Ma, Y. Lai, and S. Wang, "Transformer Structure of Bifilar Primary Winding with Advanced Common Mode Noise Attenuation Performance for Isolated DC-DC Converters," in *2023 IEEE Applied Power Electronics Conference and Exposition (APEC)*, 19-23 March 2023, pp. 441-448.

[18] R. B. Beddingfield, S. Bhattacharya, and P. Ohodnicki, "Shielding of Leakage Flux Induced Losses in High Power, Medium Frequency Transformers," in *2019 IEEE Energy Conversion Congress and Exposition (ECCE)*, 29 Sept.-3 Oct. 2019.

[19] H. Li, P. Yao, Z. Gao, and F. Wang, "Medium Voltage Converter Inductor Insulation Design Considering Grid Insulation Requirements," in *2021 IEEE Applied Power Electronics*

Conference and Exposition (APEC), 14-17 June 2021, pp. 2120-2126.

[20] J. E. Hayek and T. J. Sobczyk, "Analytic one-dimensional design method for railways traction transformers," in IEEE International Electric Machines and Drives Conference, 2003. IEMDC'03., 1-4 June 2003, vol. 3, pp. 1760-1765 vol.3.

[21] L. Li, Q. Chen, and L. Zhou, Dianci Zhuangzhi Sheji Yuanli [Design Principle of Electromagnetic Device] (in Chinese). Beijing, China: China Electric Power Press, 2017, pp. 39-41, 64-74.

[22] L. Yi and J. Moon, "In Situ Direct Magnetic Loss Measurement With Improved Accuracy for Lossier Magnetics," *IEEE Transactions on Instrumentation and Measurement,* vol. 71, pp. 1-14, 2022, Art no. 6001414.

[23] C. R. Sullivan and R. Y. Zhang, "Simplified design method for litz wire," in *2014 IEEE Applied Power Electronics Conference and Exposition - APEC 2014*, 16-20 March 2014, pp. 2667-2674.

[24] H. Neubert, J. Ziske, T. Heimpold, and R. Disselnkötter, "Homogenization Approaches for Laminated Magnetic Cores using the Example of Transient 3D Transformer Modeling," presented at the the 2013 COMSOL Conference, Rotterdam, Netherland, 2013.

[25] A. Cremasco, D. Rothmund, M. Curti, and E. A. Lomonova, "Voltage Distribution in the Windings of Medium-Frequency Transformers Operated With Wide Bandgap Devices," *IEEE Journal of Emerging and Selected Topics in Power Electronics,* vol. 10, no. 4, pp. 3587-3602, Aug. 2022.